High-temperature self-energy corrections to x-ray absorption spectra

Tun S. Tan [1,*] J. J. Kas [2] S. B. Trickey [1] and J. J. Rehr [2]

[1]*Quantum Theory Project, Department of Physics, University of Florida, Gainesville, Florida 32611, USA*
[2]*Department of Physics, University of Washington, Seattle, Washington 98195-1560, USA*

Effects of finite-temperature quasiparticle self-energy corrections on x-ray absorption spectra are investigated within the finite-temperature quasiparticle local density GW approximation up to temperatures T of order the Fermi temperature. To facilitate the calculations, we parametrize the quasiparticle self-energy using low-order polynomial fits. We show that temperature-driven decrease in the electron lifetime substantially broadens the spectra in the near-edge region with increasing T. However, the quasiparticle shift is most strongly modified near the onset of plasmon excitations.

I. INTRODUCTION

The advancement of free electron laser sources enables routine ultrafast pump-probe experiments. Electrons can be optically excited and measurements can be done at intervals much shorter than the electron-phonon relaxation time [1–9]. This enables the study of nonequilibrium states, in which the electron temperature T_e and the ion temperature T_i are quite different in extreme conditions such as very high temperatures and densities.

Various calculations of x-ray absorption spectra (XAS) at finite temperature (FT) have been carried out in recent years. These studies involve temperatures that range from low temperatures (LT) up to a few hundred K, to the warm dense matter (WDM) regime at high temperatures (HT), where T is of order the Fermi temperature T_F [2,3,10–16]. A standard LT approach is to apply Fermi's golden rule with initial and final states calculated using conventional density functional theory (DFT) and Fermi occupation factors. While the long lifetime nonthermal electrons have been observed in some experiments, the majority of the measurements in the picosecond range are well described by thermalized electrons. For the study of nonthermal electrons, see Refs. [1,5,7–9].

Since DFT is a ground-state theory, FT quasiparticle corrections to DFT are essential for HT excited-state calculations [17,18]. However, even at extreme temperatures, e.g., many thousands of K, self-consistent field calculations of the core-hole state have typically been done with ground-state exchange-correlation functionals $\varepsilon_{xc}[\rho]$ [4,11,15,19]. This ground-state approximation can be unreliable in that its validity depends strongly on the system state and its properties. Some properties are only weakly sensitive to the temperature dependence of exchange and correlation, at least for temperatures well below the WDM regime. Others, such as the electrical conductivity and x-ray absorption spectra (XAS), are strongly temperature dependent [20,21]. Even so, the use of temperature-dependent free-energy exchange-correlation

functionals $f_{xc}[\rho, T]$ [21–27] alone ignores effects such as inelastic losses. For example, the electron inelastic scattering effect, which results in an energy-dependent broadening, is often included via a postprocessing step by convolution of the absorption cross section using an empirical model (e.g., Seah-Dench formalism [28,29]), or the imaginary part of the self-energy [30]. However, the FT dependence of the energy-dependent broadening is typically neglected.

Another common approach for XAS calculations has been the use of the real-space multiple scattering (RSMS) method, which is also referred to as the real-space Green's function (RSGF) approach [31]. This approach is the real-space analog of the Korringa-Kohn-Rostoker (KKR) approach [32–36]. The method treats excited quasiparticle states via an energy-dependent self-energy, and also takes into account the dynamic response of the system to the suddenly created core hole. The self-energy can be viewed as an energy-dependent, nonlocal analog of the exchange-correlation potential in Kohn-Sham DFT [37]. The FT generalization of the self-energy can be done formally via the Matsubara formalism. For example, Benedict *et al.* [38] used the approach to investigate the effect of T on the spectral function in jellium and aluminum, e.g., on optical properties of solid-density Al. Alternatively, as discussed by Kas *et al.* [39], the FT self-energy can be calculated using a generalization of the Migdal approximation [40], analogous to the FT GW approximation of Hedin [41].

The high-temperature Green's function approach in Ref. [42] incorporates the FT Fermi occupation of the initial and final states, FT self-consistent electron density, FT exchange-correlation potential, and lattice vibration effects. However, the consequences of the FT GW self-energy for XAS (especially at extreme-state conditions) have not been explored in detail heretofore. Such effects are relevant to nonequilibrium systems in which hot electrons exist within a cold lattice for sufficiently long times to make that distinction physically meaningful. These conditions are achievable in transient pump-probe experiments.

Thus, the main goal of this work is to study the effects of the FT GW self-energy on XAS. In order to facilitate the

*tunshengtan@ufl.edu

calculations we introduce a parametrization of the quasiparticle FT GW self-energy within the G_0W_0 scheme [43]. As illustrations, we apply the approach to the XAS for two systems with T up to 5 eV (i.e., T of order 10^5 K). Our calculations demonstrate that thermal broadening due to the imaginary part of the self-energy is significant above T of a few eV. Lattice vibrations also are strongly temperature dependent, that behavior is dependent on the lattice temperature T_l, which can differ from the electronic temperature T in nonequilibrium states. The lattice vibrations strongly damp the XAS fine structure at all temperatures [42].

The remainder of the paper is organized as follows. Section II provides a brief overview of the real-space Green's function approach to XAS and its dependence on the self-energy Σ. In Sec. III, we highlight the FT corrections to XAS with a few examples and in Sec. IV we present a brief summary and conclusions. Throughout we use Hartree atomic units, $q_e = \hbar = m = 1$, with $q_e = e$ the electron charge. Thus energies are in Hartree and distances in Bohr, unless otherwise noted. For temperature we use either K or eV, with 1 eV $\approx$ 11604 K. Electron densities are expressed in Wigner-Seitz radii $r_s = (3/4\pi\rho)^{1/3}$.

II. THEORY SUMMARY

A. Finite-temperature x-ray absorption

Formally the zero-temperature x-ray absorption cross section is defined via Fermi's golden rule as

$$\sigma(\omega) = 4\pi^2 \frac{\omega}{c} \sum_{i,f} |\langle \Psi_i | \mathbf{D} | \Psi_f \rangle|^2 \delta_\Gamma(\omega + E_i - E_f), \quad (1)$$

where $|\Psi_i\rangle$ and $|\Psi_f\rangle$ are the many-body initial and final states, and $\mathbf{D} = \sum_i d_i$ is the many-body (dipole) interaction with the x-ray field. Then within the single-particle (quasiparticle) approximation with dipole interactions and the sudden approximation, the zero-temperature XAS becomes

$$\sigma_s(\omega) = 4\pi^2 \frac{\omega}{c} \sum_{i,f} |\langle i | d | f \rangle|^2 \delta_\Gamma(\omega + \varepsilon_i - \varepsilon_f), \quad (2)$$

where ε_i and ε_f are the energies of the quasiparticle initial $|i\rangle$ and final $|f\rangle$ levels and many-body shake-up factors $S_0^2 \approx 1$ are ignored. The δ_Γ factor denotes a Lorentzian of width Γ, which includes both quasiparticle and core-hole lifetime broadening. Here, the transition operator $d = \hat{\xi} \cdot \mathbf{r}$ is the single-particle electric dipole operator and $\hat{\xi}$ is the polarization of the incident photon. The one-particle states $|i\rangle$ and $|f\rangle$ can be obtained from Hartree-Fock theory or Kohn-Sham DFT. For the treatment via DFT, see, e.g., Refs. [28,44,45].

For x-ray absorption, the number of final states $|f\rangle$ required to compute the dipole matrix element has a huge impact on the computational efficiency of evaluating Eq. (2). The present work uses the RSMS approach to circumvent this bottleneck. In RSMS, the summation over the final states $|f\rangle$ is replaced with the retarded single-electron Green's function $G(\omega)$ in a basis of local site-angular momentum states $|Lj\rangle$ [31],

$$G_{LL'}^{jj'}(\omega) = \sum_f \frac{\langle Lj | f \rangle \langle f | L'j' \rangle}{\omega - \varepsilon_f + i\eta}. \quad (3)$$

In this expression, j is the index of a given site $\mathbf{R}_j$ and $L = (l, m)$ are the angular momentum quantum numbers. The initial states $|i\rangle$ are calculated with the ground-state Hamiltonian $H = p^2/2 + v(\mathbf{r}) + v_{xc}(\mathbf{r}) + v_{ie}(\mathbf{r})$ while the final states $|f\rangle$ are described by the quasiparticle Hamiltonian $H' = p^2/2 + v_f(\mathbf{r}) + \Sigma(\mathbf{r}, E) + v_{ie}(\mathbf{r})$, where v is the self-consistent one-electron Hartree potential, v_{xc} is the exchange-correlation potential, v_{ie} is the electron-ion potential, v_f is the final-state one-electron Hartree potential in the presence of a screened core hole, and Σ is the dynamically screened quasiparticle self-energy discussed in detail below. The exchange-correlation v_{xc} is sufficient to give a good approximation to the quasiparticle ground state (initial state).

The imaginary part of the quasiparticle self-energy Σ accounts for the mean-free path of the photoelectron. Within the quasiparticle local density approximation (QPLDA) [46], the self-energy is given by [47]

$$\Sigma(\mathbf{r}, E, T = 0) = v_{xc}^{LDA}(\rho(\mathbf{r})) + \Sigma_{GW}(\rho(\mathbf{r}), E, T = 0)$$
$$- \Sigma_{GW}(\rho(\mathbf{r}), E_F, T = 0). \quad (4)$$

Here Σ_{GW} is the GW self-energy calculated at the G_0W_0 level of refinement, that is, without self-consistent iteration of G or W [41]. For simplicity from here onward, we drop the spatial dependence $\mathbf{r}$.

For the FT generalization, we replace the $T = 0$ GW self-energy with the finite-temperature GW self-energy, $\Sigma_{GW}(T)$, and introduce T-dependent Fermi occupation numbers, $f(\varepsilon) = 1/[\exp\{\beta(\varepsilon - \mu)\} + 1]$ for the initial and final states in Eq. (2). In addition, the ground-state exchange-correlation potential v_{xc}^{LDA} is replaced by its FT generalization $v_{xc}^{LDA}(T)$. Thus, the finite-temperature QPLDA self-energy is

$$\Sigma(E, T) = v_{xc}^{LDA}(\rho, T) + \Sigma_{GW}(\rho, E, T)$$
$$- \text{Re}\left[\Sigma_{GW}(\rho, \mu_T, T)\right]. \quad (5)$$

Lastly, by using $G_{LL'}^{jj'}(\omega)$ in Eq. (2) in place of the sum over final states $|f\rangle$, the FT quasiparticle cross section can be reexpressed as [48]:

$$\sigma_{qp}(\omega) = -4\pi^2 \frac{\omega}{c} \text{Im} \sum_{iLL'} \langle i | \hat{d} G_{LL'}^{00}(\omega + \varepsilon_i) \hat{d}^\dagger | i \rangle$$
$$\times f(\varepsilon_i)[1 - f(\omega + \varepsilon_i)], \quad (6)$$

Here we denote the absorbing atom by the index 0.

B. Finite-temperature self-energy Σ

The finite-T quasiparticle electron self-energy within the GW approximation is defined formally [40,49] by the expression

$$\Sigma_{GW}^M(\mathbf{k}, i\omega_m) = -\frac{1}{\beta} \int \frac{d^3q}{(2\pi)^3} \sum_{n=-\infty}^{\infty} G_0^M(\mathbf{k} - \mathbf{q}, i\omega_m - i\nu_n)$$
$$\times W^M(\mathbf{q}, i\nu_n). \quad (7)$$

Here G_0^M is the one-electron Matsubara Green's function, $W^M = \epsilon^{-1}v$ is the screened Coulomb interaction, and $\omega_m = 2(m + 1)\pi k_B T$, $\nu_n = 2n\pi k_B T$ are the Matsubara frequencies, while ϵ is the dielectric function and v is the bare Coulomb potential. The screened interaction W^M can be expressed in

terms of its spectral representation as

$$W^M(\mathbf{q}, i\nu_n) = v(\mathbf{q}) + \int_{-\infty}^{\infty} d\omega' \frac{D(\mathbf{q}, \omega')}{i\nu_n - \omega' + i\eta \, \text{sgn}(\omega')}, \quad (8)$$

where $v(\mathbf{q}) = 4\pi/q^2$ is the bare Coulomb potential in Fourier representation, and $D(\mathbf{q}, \omega) = (1/\pi)|\text{Im } W_c^M(\mathbf{q}, \omega)| \, \text{sgn}(\omega)$ is the antisymmetric (in frequency) bosonic excitation spectrum. $W_c^M = W^M - v$ is the correlation part of the screened interaction.

Next, we approximate the exact dielectric function with the uniform electron gas model. Our choice of the electron gas dielectric function reflects a balance between the level of physics included and computational feasibility. Thus, for simplicity, we use the random phase approximation (RPA), which is analogous to the FT generalization of the Lindhard function [50],

$$\epsilon(\mathbf{q}, \omega, T) = 1 + 2v(\mathbf{q}) \int \frac{d^3k}{(2\pi)^3} \frac{f(\varepsilon_{\mathbf{k}-\mathbf{q}}) - f(\varepsilon)}{\omega - \varepsilon_{\mathbf{k}-\mathbf{q}} + \varepsilon_{\mathbf{k}} + i\eta}, \quad (9)$$

where $f(\varepsilon) = 1/[\exp\{\beta(\varepsilon - \mu)\} + 1]$ is the Fermi-Dirac occupation factor, and $\mu = \mu(T)$ is the chemical potential. The real part of $\epsilon(\mathbf{q}, \omega, T)$ is obtained from the imaginary part via a Kramers-Kronig transform. From an analytic continuation to the real-ω axis, the FT GW retarded self-energy Σ_{GW} is given by the Migdal approximation [40]

$$\Sigma_{GW}(\mathbf{k}, \omega, T) = \Sigma_X(\mathbf{k}, \omega, T) + \int_0^{\infty} d\omega' \int \frac{d^3q}{(2\pi)^3} D(\mathbf{q}, \omega')$$

$$\times \left[\frac{f(\varepsilon_{\mathbf{k}-\mathbf{q}}) + N(\omega')}{\omega + \omega' - \varepsilon_{\mathbf{k}-\mathbf{q}} + i\eta} + \frac{1 - f(\varepsilon_{\mathbf{k}-\mathbf{q}}) + N(\omega')}{\omega - \omega' - \varepsilon_{\mathbf{k}-\mathbf{q}} + i\eta} \right], \quad (10)$$

where $\Sigma_X(\mathbf{k}, \omega, T) = \int[d^3q/(2\pi)^3]f(\varepsilon_{\mathbf{k}-\mathbf{q}})v_{\mathbf{q}}$ is the exchange part of the self-energy and $N(\omega) = 1/[\exp\{\beta\omega\} - 1]$ is the Bose factor. The poles of the Green's function G^M contribute to the Fermi occupations whereas the poles of the screened interaction W^M contribute to the Bose factor.

Calculations of the imaginary part of $\Sigma_{GW}(\mathbf{k}, \omega, T)$ involve a single integral over the magnitude of $\mathbf{q}$. But to obtain the real part, we need to perform a Kramers-Kronig transform resulting in a double integral. In typical RSGF XAS calculations [51], tens of thousands of self-energy evaluations are required. Thus that calculation of quasiparticle self-energy $\Sigma_{GW}(k, k^2/2, T)$ becomes a major computational bottleneck. To circumvent that difficulty, we model $\Sigma_{GW}(k, k^2/2, T)$ via low-order polynomial fits to numerical calculation of Σ_{GW} based on Eq. (10), on a grid up to $T = 2 T_F$, where $T_F = E_F/k_B$. The form of the fitting functions is described in detail in the Appendixes. A comparison between the QPLDA Σ_{GW} and the fits is shown in Fig. 1 for the homogeneous electron gas. For simplicity, we approximate the self-energy for levels $k < k_F$ with $v_{xc}(T)$ independent of k.

III. RESULTS AND DISCUSSION

Results presented in this section show effects of using the FT $\Sigma_{GW}(T > 0)$ instead of the zero T values $\Sigma_{GW}(T = 0)$. Note that $\Sigma_{GW}(T = 0)$ depends implicitly on the electronic temperature T_e through the self-consistent electron density at that temperature. The FT SCF calculations are carried out
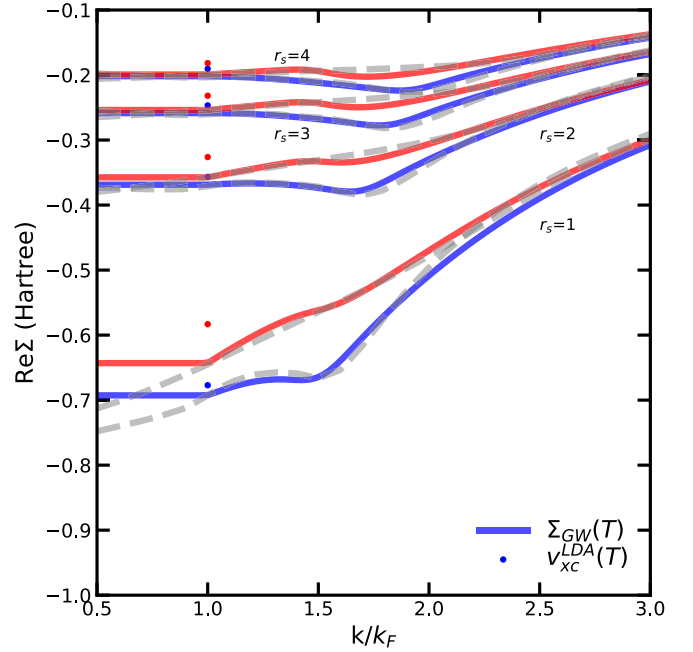

FIG. 1. The real part of the Σ_{GW} (dashed) and our parametrization (solid) for various densities: r_s=1.0, 2.0, 3.0, 4.0 at T/T_F=0.01 (blue) and 1.0 (red). For reference the LDA-v_{xc}(T) [26] values are denoted as dots at k_F.

using an extension of the original RSMS code, which now is implemented in FEFF10 [51,52]. For the FT exchange correlation potential, we use the KSDT tabulation $v_{xc}^{LDA}(T)$ [26,53] for both calculations. The Fermi temperature T_F used in this section is defined based on the electron gas model with a density equal to the interstitial density $\rho_{\text{int}} = 3/4\pi r_{s,\text{int}}^3$ of the system under consideration. In the FEFF10 calculations, we compute the atomic part using $\Sigma_{GW}(\rho = \rho_{\text{int}}, E = \mu_T, T)$ and the fine structure using $\Sigma_{GW}(T)$.

The relaxation of core states is important in the case of warm dense matter [11,15]. The shifts in the core energy levels become significant when $T \gtrsim 1$ eV. However, the frozen core approximation is used in FEFF10. Therefore, we estimate the core level shifts in our calculations by use of the all-electron full-potential linearized plane wave code FLEUR [54–56]. Within those calculations, we ignore the explicit temperature dependence in the LDA exchange correlation functional [57]. As a side note, FLEUR uses nonoverlapping muffin-tin potentials whereas FEFF uses overlapping muffin-tin potentials.

In the RSMS formalism, the decomposition of the Green's function G into a central atom G^c contribution and a multiple-scattering G^{sc} contribution allows us to describe the XAS in terms of the atomic background σ_0 and the oscillatory fine structure χ, i.e., $\sigma = \sigma_0(1 + \chi)$. For many XANES calculations, it is found that the atomic background matches the experimental results better when calculated without the self-energy corrections due to the overestimation of the exchange within the muffin-tin (MT) potential approximation [58]. Figure 2 shows the effect of using different exchange-correlation potentials for the atomic background. When using
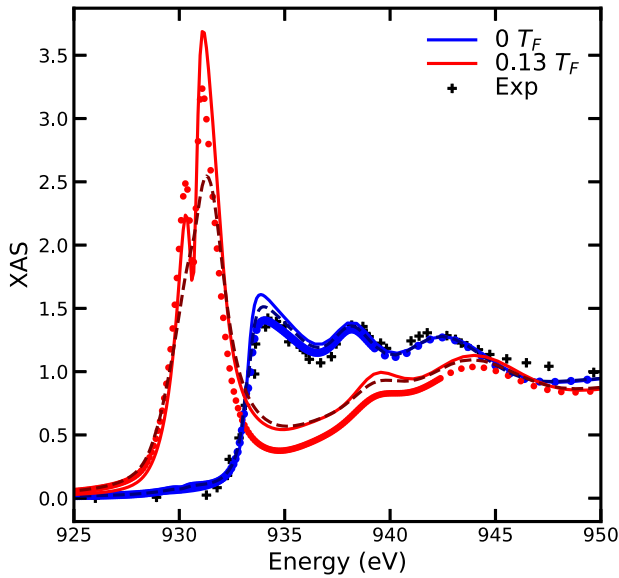
FIG. 2. L_3-edge XAS for Cu (lattice constant $a = 3.61$ Å [59]) at electronic temperature $T = 0.025$ eV ≈ 0 T_F and $T = 0.13$ $T_F = 2$ eV. Different atomic background potentials are used: ground-state potential (solid), $\Sigma_{GW}(T)$ (dots), and constant potential $\Sigma_{GW}(\rho = \rho_{\text{int}}, E = \mu_T, T)$ (dashes). The experimental measurement at ambient conditions is shown as black cross [60].

FIG. 3. K-edge XAS for fcc aluminum ($a = 4.05$ Å) using different self-energies: T-independent GW self-energy $\Sigma_{GW}(T = 0)$ (solid curves) and T-dependent GW self-energy $\Sigma_{GW}(T > 0)$ (dots) for $T = 0$, 0.08, 0.16, and 0.42 T_F.

$\Sigma_{GW}(T)$, the absorption near the edge is overestimated. At the same time, use of a ground-state potential neglects the temperature dependence in the atomic background. To remedy the problem, we introduce a constant effective potential for the atomic background $\Sigma_{GW}(\rho = \rho_{\text{int}}, E = \mu_T, T)$. Our modification also improves the agreement with the experimental measurement at low temperature $T \approx 0$ T_F.

For brevity from here onward, we refer to the combination of $\Sigma_{GW}(\rho = \rho_{\text{int}}, E = \mu_T, T)$ for the atomic background and $\Sigma_{GW}(T)$ for the fine structure simply as $\Sigma_{GW}(T)$. The pre-edge is dominated by the atomic background and thus is sensitive to the choice of exchange potential. At $T = 0.13$ $T_F = 2$ eV, the pre-edge amplitude is reduced by $\approx 30\%$ due to the temperature correction of $\Sigma_{GW}(T)$. More pump-probe experimental XAS measurements for $T \approx T_F$ are required to validate the FT self-energy effect for the atomic background. Nonetheless, the FT self-energy corrections are important for the description of HT fine structure.

As a first example, we consider the FT K-edge x-ray absorption near-edge spectrum (XANES) for aluminum (fcc Al, lattice constant $a = 4.05$ Å [59]). Aluminum is a prototypical nearly free electron system in the sense that the electronic density of states (DOS) in the conduction band has a nearly square-root-like dispersion at the bottom of the band. Figure 3 shows the comparison of the Al K-edge spectrum at different temperatures including or excluding explicit electronic T-dependent effects in the self-energy, namely, using $\Sigma_{GW}(T = 0)$ or $\Sigma_{GW}(T > 0)$. When restricting the temperature T solely to that which is introduced through the density [$\Sigma_{GW}(T = 0)$ case], we observe the broadening of the edge and almost no shift in the edge position. The decrease in occupation of the $3p$ final states below the chemical potential in the K-edge transition $1s \rightarrow 3p$ leads to
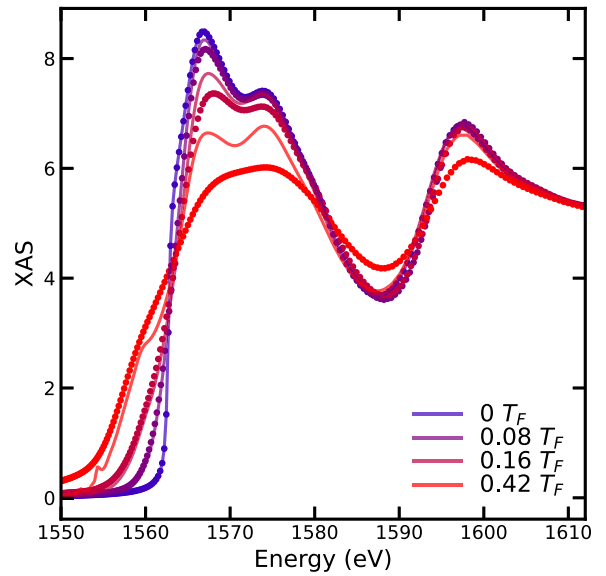
increasing pre-edge absorption and edge broadening [11,42]. In addition, the thermal excitation of the valence electron changes the valence occupation, resulting in a blue shift of the valence energy levels because there are more unoccupied states above the chemical potential. The relaxation of the core level compensates for the shift in the valence density [11]. On the other hand, for T up to about 0.08 $T_F = 1$ eV, the finite-temperature self-energy correction is negligible, and the temperature-independent electron self-energy model is a good approximation. However, as temperature grows to order ≈ 0.42 $T_F = 5$ eV, the fine structure is smoothed by the large broadening (≈ 3 eV) associated with shortened electronic excitation lifetime. The shift in quasiparticle energy due to the finite-temperature self-energy correction is small for the near-edge region, and only becomes significant between 10 eV and 20 eV above the chemical potential.

As a further illustration of the explicit T dependence of the FT quasiparticle self-energy, we compute the quasiparticle energy correction $\Delta_k = \varepsilon_{qp} - \varepsilon_k$ at $r_{s,\text{int}}$. Here, the quasiparticle energy ε_{qp} is the solution to $\varepsilon_{qp}(k') = \varepsilon_k + \Sigma[k', \varepsilon_{qp}(k')]$ and $k = \sqrt{2(E - \mu_T)}$ is the photoelectron wave number. We compare the real part of Δ in Fig. 4 and imaginary part in Fig. 5 for different self-energies at $r_{s,\text{int}}$: $\Sigma_{GW}(T = 0)$ and $\Sigma_{GW}(T > 0)$. Note that the real part of Δ shows a strong temperature dependence between 5 eV and 20 eV near the plasmon onset. For the imaginary part of Δ, the broadening effect becomes important above $T = 0.08$ $T_F = 1$ eV.

As a second example, we present results for a noble transition metal (fcc copper, lattice constant $a = 3.61$ Å [59]) for which the d bands are essentially full. Unlike the K edge, the L edge probes the highly localized d bands of Cu near the chemical potential. At high temperatures, the pre-edge peak increases in amplitude due to the decreasing d-state occupation [15,42]. Figure 6 shows the $L_{3,2}$-edge XAS up to $T = 0.30$ $T_F = 5$ eV. Unlike the Al K-edge case, the
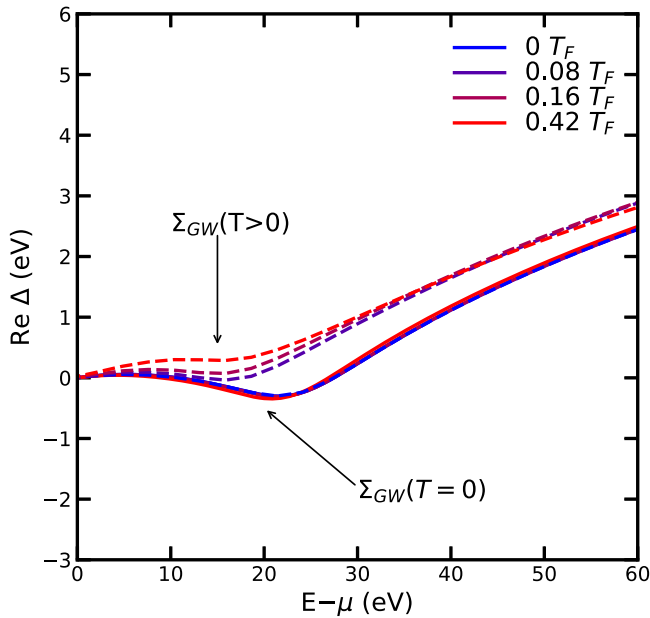
FIG. 4. The quasiparticle corrections Re Δ_k for aluminum at temperatures $T = 0, 0.08, 0.16,$ and $0.42\ T_F$. The calculations used KSDT $v_{xc}(T)$ and different self-energies: $\Sigma_{GW}(T = 0)$ (solid), and $\Sigma_{GW}(T > 0)$ (dashed).

$L_{3,2}$-edge transition $2p \rightarrow 3d$ has two peaks near 935 eV and 955 eV due to the spin-orbit splitting. These correspond to the $2p_{3/2} \rightarrow 3d_{5/2}$ and $2p_{1/2} \rightarrow 3d_{3/2}$ transitions. Ignoring the temperature dependence of Σ, the absorption edge is sensitive to the change in occupation as a function of temperature because the highly localized d bands of Cu are below the chemical potential. The pre-edge peak near 930 eV increases as electron occupation below the chemical potential decreases with temperature.
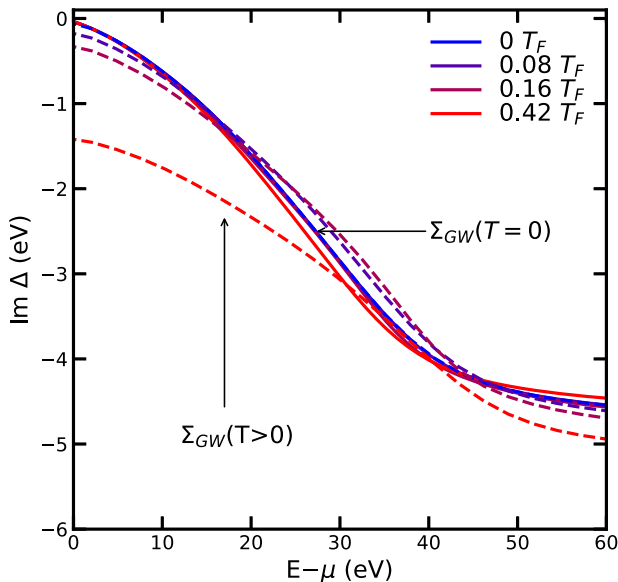

FIG. 5. The quasiparticle corrections Im Δ_k for aluminum at temperatures $T = 0, 0.08, 0.16,$ and $0.42\ T_F$. The calculations used KSDT $v_{xc}(T)$ and different self-energies: $\Sigma_{GW}(T = 0)$ (solid), and $\Sigma_{GW}(T > 0)$ (dashed).
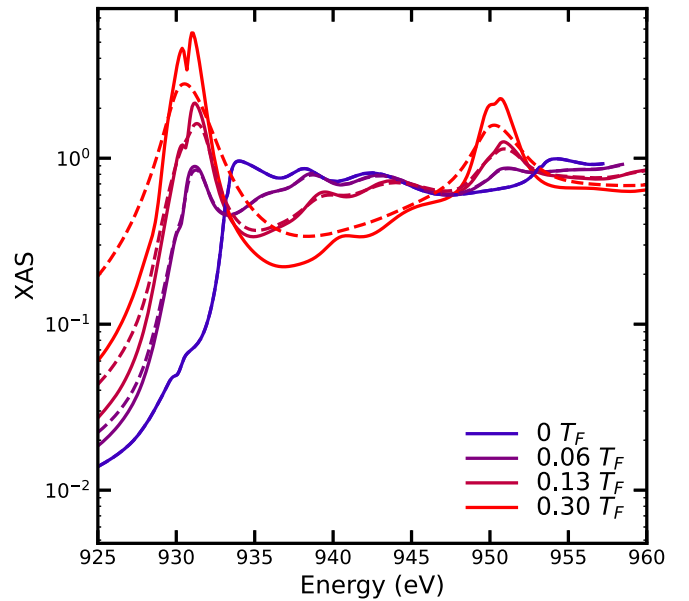

FIG. 6. $L_{3,2}$-edge XAS for Cu ($a = 3.61$ Å) finite electronic temperature $T = 0, 0.06, 0.14$ and $0.30\ T_F$, where the structure reflects that of the unfilled d bands. The solid curves denote the $\Sigma_{GW}(T = 0)$ self-energy results while the dashes represent the $\Sigma_{GW}(T > 0)$ self-energy results.

The temperature dependence of Im $\Sigma_{GW}(T)$ results in changes to pre-edge peaks at $T \gtrsim 0.13\ T_F = 2$ eV. Consequently, the estimation of temperature based on the pre-edge area method or direct spectrum fitting will deviate more from the $\Sigma_{GW}(T = 0)$ model as temperature increases.

IV. SUMMARY, CONCLUSIONS, AND OUTLOOK

Our parametrization of the FT GW electron self-energy enables efficient calculations of XAS at finite T, from LT of a few hundred K, up to the WDM regime with T at least 10 eV. Our strategy uses the QPLDA G_0W_0 level of refinement for the self-energy, with the RPA dielectric function in conjunction with the KSDT finite-T LDA exchange-correlation functional. Specifically, the FT self-energy for a system is approximated using the uniform electron gas with density equal to that of the local density. This is a significant simplification, as direct calculations using the exact loss function of the system for the entire energy range of typical XAS experiments would be computationally formidable. A finite-temperature SCF procedure for the XAS calculations is carried out in the complex energy plane in terms of the FT one-electron Green's function. The procedure includes the FT exchange-correlation potential, approximated here by the KSDT parametrization. Important FT XAS effects include the smearing of the absorption edge and the presence of peaks in the spectrum below the $T = 0$ K Fermi energy. The FT exchange-correlation potential has only a small effect on XAS at low temperatures $T \ll T_F$ compared to the effect of Fermi smearing. The FT self-energy is also important for XAS, accounting for both temperature-dependent shifts and final-state broadening. To illustrate its efficacy, the approach was applied to calculations of XANES for crystalline Al and Cu at normal density. Above

$T > 0.1 \, T_F$, the fine structures experience substantial broadening in the K edges, corresponding to a reduction of the quasiparticle lifetime with increasing T.

Going forward, a computationally efficient approximation beyond the uniform electron gas dielectric function would be to use a many-pole model [61,62], which is an extension of the Hedin-Lundqvist single plasmon-pole model [63,64]. *Ab initio* dielectric functions also can be obtained from modern electronic structure codes. Such a finite-temperature generalization of the many-pole model is currently under development.

APPENDIX A: MODEL FOR Re Σ_{GW}

The real part of the finite-temperature GW self-energy, Re $\Sigma_{GW}(T)$, is parametrized using low-order polynomials. The parametric variables are the Wigner-Seitz radius r_s, reduced momentum $x = k/k_F$, and reduced temperature $t = T/T_F$. Below the variable X represents the array denoted $X = (r_s, x, t)$.

$$\frac{\text{Re } \Sigma_{GW}(X)}{E_F} = \begin{cases} \alpha_0(t) + \alpha_1(t)\beta_1(r_s)x \\ + \alpha_2(t)\beta_2(r_s)x^{3/2} \\ + \alpha_3(t)\beta_3(r_s)x^2 \\ + \alpha_4(t)\beta_4(r_s)x^{5/2}, & x < \kappa(r_s, t) \\ \tilde{\alpha}_1(t)\tilde{\beta}_1(t)x^{-1} \\ + \tilde{\alpha}_2(t)\tilde{\beta}_2(t)x^{-2} \\ + \tilde{\alpha}_3(t)\tilde{\beta}_3(t)x^{-3}, & x \geqslant \kappa(r_s, t) \end{cases} \quad \text{(A1)}$$

Here $\alpha_i(t) = \alpha_{i1} + \alpha_{i2}t + \alpha_{i3}t^2$ and $\tilde{\alpha}_i(t)$ has the same form. Similarly $\beta_i(r_s) = \beta_{i1}r_s + \beta_{i1}r_s^{3/2} + \beta_{i1}r_s^2$ and $\tilde{\beta}_i(r_s)$ has the same form. The function κ is defined as:

$$\kappa(r_s, t) = (1 + \tanh[a_1 r_s - \alpha_1(t)]) \\ \times (a_2 \log[r_s]^2 + \alpha_2(t)) + \alpha_3(t), \quad \text{(A2)}$$

where it is fitted to the position of the cusp defined as

$$\text{cusp} = \begin{cases} \min(1.5, \arg\min_x \text{Re } \Sigma_{GW}), & 0.2 < r_s \leqslant 5 \\ \min(1.5, \arg\max_x \partial_x \text{Re } \Sigma_{GW}), & r_s > 5 \\ 1, & r_s \leqslant 0.2 \end{cases} \quad \text{(A3)}$$

The resulting Re Σ_{GW} parametrization is shown in Fig. 7. The absolute mean error for our parametrization is $\approx 0.007 \, E_F$. A list of the parameters in these fits is given in the Supplemental Material [65].
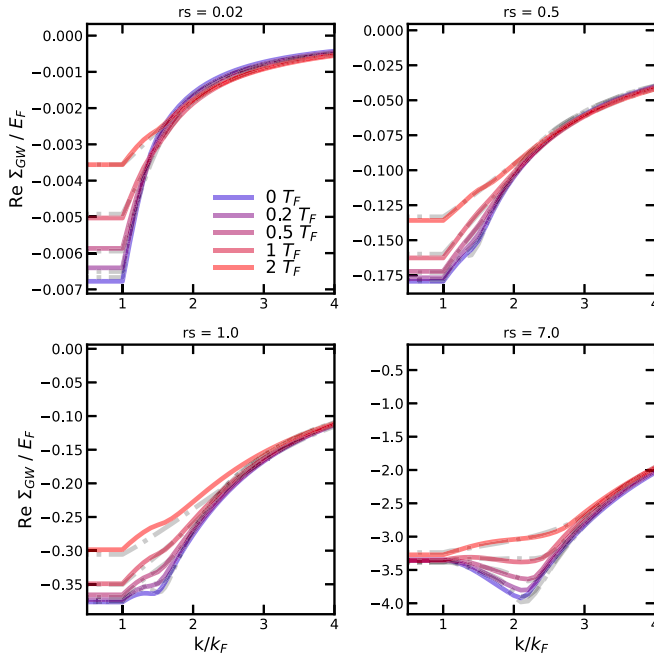

FIG. 7. Our parametrization (solid) to the real part of $\Sigma_{GW}(T)$ (gray, dash-dotted) for $r_s = 0.02$, 0.5, 1.0, and 7.0 (blue to red).
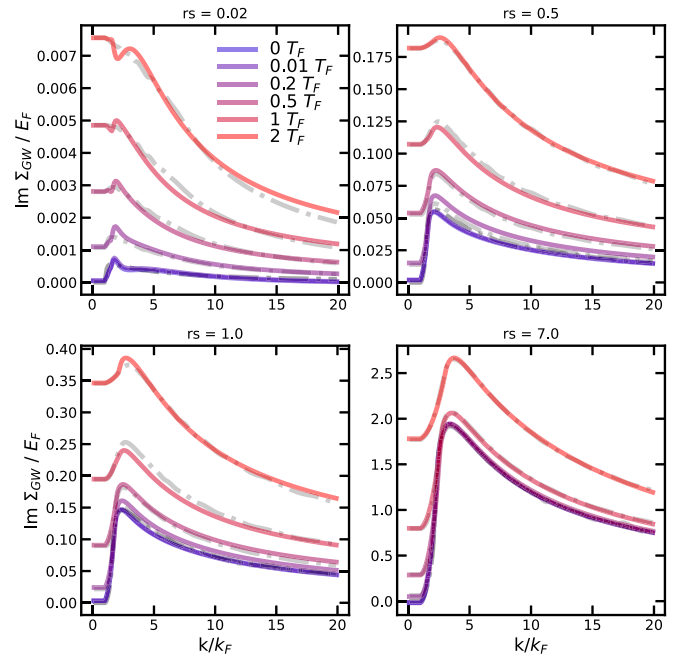

FIG. 8. Our parametrization (solid) to the imaginary part of $\Sigma_{GW}(T)$ (gray, dash-dotted) for $r_s = 0.02$, 0.5, 1.0, and 7.0 (blue to red).

APPENDIX B: MODEL FOR Im Σ_{GW}

The imaginary part of the finite-temperature *GW* self-energy, Im $\Sigma_{GW}(T)$, is parametrized by

$$\frac{\text{Im }\Sigma_{GW}(X)}{E_F} = \begin{cases} \eta_1(r_s)xt + \eta_2(r_s)xt^{\frac{3}{2}} \\ +\eta_3(r_s)x^2t + \eta_4(r_s)x^2t^{\frac{3}{2}} \\ +\eta_5(r_s)x^{\frac{3}{2}}t + \eta_6(r_s)x^{\frac{3}{2}}t^{\frac{3}{2}} \\ +\eta_7(r_s)x + \eta_8(r_s)x^2 \\ +\eta_9(r_s)x^{\frac{3}{2}} \\ +\frac{\text{Im }\Sigma_{GW}(r_s,x=1,t)}{E_F}, & x < \lambda(r_s,t) \\ \sigma\left(\sum_{i=1}^5 \tilde{\eta}_i(r_s)\beta_i(t)x^{-i}\right. \\ \left.+\tilde{\eta}_6(r_s)\beta_6(t)x^{-1/2}\right), & x \geqslant \lambda(r_s,t) \end{cases}, \quad \text{(B1)}$$

where $\eta_i(r_s)$, $\tilde{\eta}(r_s) = \eta_{i1}r_s + \eta_{i2}r_s^{3/2} + \eta_{i3}r_s^2$ and σ is the standard deviation of the data points used. The function $\lambda(r_s, t)$ is given by

$$\lambda(r_s, t) = \left(1 + \tanh\left[\frac{r_s - \frac{1}{2}}{p_1}\right]\right)(p_2 r_s + \eta_1(t)) + \eta_2(t) \quad \text{(B2)}$$

and Im Σ at the Fermi level, k_F, is parametrized by:

$$\frac{\text{Im }\Sigma_{GW}(r_s, x = 1, t)}{E_F} = \nu_1(t)r_s^{\frac{1}{2}} + \nu_2(t)r_s + \nu_3(t)r_s^{\frac{3}{2}}, \quad \text{(B3)}$$

where $\nu_i(t) = \nu_{i1}t + \nu_{i2}t^{3/2} + \nu_{i3}t^2$. The fittings of Eq. (B1), Eq. (B2), and Eq. (B3) are done for two temperature regions: $t < 0.5$ and $t \geqslant 0.5$, and two density regions: $r_s < 0.2$ and $r_s \geqslant 0.2$.

The final model is a linear combination of the left and right regions in Eq. (B1). The left region is weighted by the Fermi function $w = 1/\{1 + \exp[15(k - 1.1\lambda(r_s, t))]\}$ and the right side by $1 - w$. In addition, to prevent spurious negative values at very low t, we clip any negative values to be zero. The resulting parametrization is shown in Fig. 8. The absolute mean error for our parametrization is $\approx 0.006\,E_F$. A list of the parameters in these fits is given in the Supplemental Material [65].

[1] N. Medvedev, U. Zastrau, E. Förster, D. O. Gericke, and B. Rethfeld, Phys. Rev. Lett. **107**, 165003 (2011).

[2] B. I. Cho, K. Engelhorn, A. A. Correa, T. Ogitsu, C. P. Weber, H. J. Lee, J. Feng, P. A. Ni, Y. Ping, A. J. Nelson, D. Prendergast, R. W. Lee, R. W. Falcone, and P. A. Heimann, Phys. Rev. Lett. **106**, 167601 (2011).

[3] K. Engelhorn, V. Recoules, B. I. Cho, B. Barbrel, S. Mazevet, D. M. Krol, R. W. Falcone, and P. A. Heimann, Phys. Rev. B **91**, 214305 (2015).

[4] B. I. Cho, T. Ogitsu, K. Engelhorn, A. A. Correa, Y. Ping, J. W. Lee, L. J. Bae, D. Prendergast, R. W. Falcone, and P. A. Heimann, Sci. Rep. **6**, 18843 (2016).

[5] F. Bisio, E. Principi, M. Magnozzi, A. Simoncig, E. Giangrisostomi, R. Mincigrucci, L. Pasquali, C. Masciovecchio, F. Boscherini, and M. Canepa, Phys. Rev. B **96**, 081119(R) (2017).

[6] E. Principi, E. Giangrisostomi, R. Mincigrucci, M. Beye, G. Kurdi, R. Cucini, A. Gessini, F. Bencivenga, and C. Masciovecchio, Phys. Rev. B **97**, 174107 (2018).

[7] M. X. Na, F. Boschini, A. K. Mills, M. Michiardi, R. P. Day, B. Zwartsenberg, G. Levy, S. Zhdanovich, A. F. Kemper, D. J. Jones, and A. Damascelli, Phys. Rev. B **102**, 184307 (2020).

[8] M. Kim, J. H. Jung, S. H. Yang, M. S. Cho, G. Kang, G. Lee, J.-W. Lee, S. Lee, J. Sohn, and B. I. Cho, Appl. Surf. Sci. **561**, 150073 (2021).

[9] J.-W. Lee, M. Kim, G. Kang, S. M. Vinko, L. Bae, M. S. Cho, H.-K. Chung, M. Kim, S. Kwon, G. Lee, C. H. Nam, S. H. Park, J. H. Sohn, S. H. Yang, U. Zastrau, and B. I. Cho, Phys. Rev. Lett. **127**, 175003 (2021).

[10] O. Peyrusse, J. Phys.: Condens. Matter **20**, 195211 (2008).

[11] V. Recoules and S. Mazevet, Phys. Rev. B **80**, 064110 (2009).

[12] F. Dorchies, V. Recoules, J. Bouchet, C. Fourment, P. M. Leguay, B. I. Cho, K. Engelhorn, M. Nakatsutsumi, C. Ozkan, T. Tschentscher, M. Harmand, S. Toleikis, M. Störmer, E. Galtier, H. J. Lee, B. Nagler, P. A. Heimann, and J. Gaudin, Phys. Rev. B **92**, 144201 (2015).

[13] T. Ogitsu, A. Fernandez-Panella, S. Hamel, A. A. Correa, D. Prendergast, C. D. Pemmaraju, and Y. Ping, Phys. Rev. B **97**, 214203 (2018).

[14] R. Bolis, J.-A. Hernandez, V. Recoules, M. Guarguaglini, F. Dorchies, N. Jourdain, A. Ravasio, T. Vinci, E. Brambrink, N. Ozaki, J. Bouchet, F. Remus, R. Musella, S. Mazevet, N. J. Hartley, F. Guyot, and A. Benuzzi-Mounaix, Phys. Plasmas **26**, 112703 (2019).

[15] N. Jourdain, V. Recoules, L. Lecherbourg, P. Renaudin, and F. Dorchies, Phys. Rev. B **101**, 125127 (2020).

[16] Z. Li, W.-J. L. Li, C. Wang, D. Li, W. Kang, X.-T. He, and P. Zhang, Chin. Phys. B **30**, 057102 (2021).

[17] S. V. Faleev, M. van Schilfgaarde, T. Kotani, F. Léonard, and M. P. Desjarlais, Phys. Rev. B **74**, 033101 (2006).

[18] P. Hollebon, O. Ciricosta, M. P. Desjarlais, C. Cacho, C. Spindloe, E. Springate, I. C. E. Turcu, J. S. Wark, and S. M. Vinko, Phys. Rev. E **100**, 043207 (2019).

[19] A. Denoeud, A. Benuzzi-Mounaix, A. Ravasio, F. Dorchies, P. M. Leguay, J. Gaudin, F. Guyot, E. Brambrink, M. Koenig, S. Le Pape, and S. Mazevet, Phys. Rev. Lett. **113**, 116404 (2014).

[20] V. V. Karasiev, L. Calderín, and S. B. Trickey, Phys. Rev. E **93**, 063207 (2016).

[21] V. V. Karasiev, J. W. Dufty, and S. B. Trickey, Phys. Rev. Lett. **120**, 076401 (2018).

[22] S. Ichimaru, H. Iyetomi, and S. Tanaka, Phys. Rep. **149**, 91 (1987).

[23] S. Tanaka, Contrib. Plasma Phys. **57**, 126 (2017).

[24] S. Tanaka, J. Chem. Phys. **145**, 214104 (2016).

[25] F. Perrot and M. W. C. Dharma-wardana, Phys. Rev. B **62**, 16536 (2000).

[26] V. V. Karasiev, T. Sjostrom, J. Dufty, and S. B. Trickey, Phys. Rev. Lett. **112**, 076403 (2014).

[27] S. Groth, T. Dornheim, T. Sjostrom, F. D. Malone, W. M. C. Foulkes, and M. Bonitz, Phys. Rev. Lett. **119**, 135001 (2017).

[28] O. Bunău and M. Calandra, Phys. Rev. B **87**, 205105 (2013).

[29] M. P. Seah and W. A. Dench, Surf. Interface Anal. **1**, 2 (1979).

[30] S. K. Cushing, M. Zürch, P. M. Kraus, L. M. Carneiro, A. Lee, H.-T. Chang, C. J. Kaplan, and S. R. Leone, Struct. Dyn. **5**, 054302 (2018).

[31] J. J. Rehr and R. C. Albers, Rev. Mod. Phys. **72**, 621 (2000).

[32] J. Korringa, Physica **13**, 392 (1947).

[33] W. Kohn and N. Rostoker, Phys. Rev. **94**, 1111 (1954).

[34] T. H. Dupree, Ann. Phys. (NY) **15**, 63 (1961).

[35] J. L. Beeby and S. F. Edwards, Proc. R. Soc. London A **302**, 113 (1967).

[36] G. J. Morgan, Proc. Phys. Soc. **89**, 365 (1966).

[37] M.E. Casida, Phys. Rev. A **51**, 2005 (1995).

[38] L. X. Benedict, C. D. Spataru, and S. G. Louie, Phys. Rev. B **66**, 085116 (2002).

[39] J. J. Kas and J. J. Rehr, Phys. Rev. Lett. **119**, 176403 (2017).

[40] P. B. Allen and B. Mitrović, in *Solid State Physics*, edited by H. Ehrenreich, F. Seitz, and D. Turnbull (Academic Press, London, 1982), Vol. 37, pp. 1–92.

[41] L. Hedin, Phys. Rev. **139**, A796 (1965).

[42] T. S. Tan, J. J. Kas, and J. J. Rehr, Phys. Rev. B **104**, 035144 (2021).

[43] R. M. Martin, L. Reining, and D. M. Ceperley, *Interacting Electrons: Theory and Computational Approaches* (Cambridge University Press, Cambridge, 2016).

[44] M. Taillefumier, D. Cabaret, A.-M. Flank, and F. Mauri, Phys. Rev. B **66**, 195107 (2002).

[45] C. Gougoussis, M. Calandra, A. P. Seitsonen, and F. Mauri, Phys. Rev. B **80**, 075102 (2009).

[46] L. J. Sham and W. Kohn, Phys. Rev. **145**, 561 (1966).

[47] J. Mustre de Leon, J. J. Rehr, S. I. Zabinsky, and R. C. Albers, Phys. Rev. B **44**, 4146 (1991).

[48] A. L. Ankudinov, B. Ravel, J. J. Rehr, and S. D. Conradson, Phys. Rev. B **58**, 7565 (1998).

[49] G. Mahan, *Many-Particle Physics* (Springer, Berlin, 2000).

[50] N. R. Arista and W. Brandt, Phys. Rev. A **29**, 1471 (1984).

[51] J. J. Kas, F. D. Vila, C. D. Pemmaraju, T. S. Tan, and J. J. Rehr, J. Synchrotron Radiat. **28**, 1801 (2021).

[52] J. J. Rehr, J. J. Kas, F. D. Vila, M. P. Prange, and K. Jorissen, Phys. Chem. Chem. Phys. **12**, 5503 (2010).

[53] V. V. Karasiev, S. B. Trickey, and J. W. Dufty, Phys. Rev. B **99**, 195134 (2019).

[54] The FLEUR code (version max-6.0): www.flapw.de.

[55] M. Weinert, E. Wimmer, and A. J. Freeman, Phys. Rev. B **26**, 4571 (1982).

[56] U. Alekseeva, G. Michalicek, D. Wortmann, and S. Blügel, in *Euro-Par 2018: Parallel Processing*, edited by M. Aldinucci, L. Padovani, and M. Torquati (Springer International Publishing, Cham, 2018), pp. 735–748.

[57] J. P. Perdew and A. Zunger, Phys. Rev. B **23**, 5048 (1981).

[58] J. J. Rehr, C. H. Booth, F. Bridges, and S. I. Zabinsky, Phys. Rev. B **49**, 12347 (1994).

[59] C. Kittel, in *Introduction to Solid State Physics*, 8th ed. (Wiley, Hoboken, 2005), p. 20.

[60] S. Kiyono, S. Chiba, Y. Hayasi, S. Kato, and S. Mochimaru, Jpn. J. Appl. Phys. **17**, 212 (1978).

[61] J. J. Kas, A. P. Sorini, M. P. Prange, L. W. Cambell, J. A. Soininen, and J. J. Rehr, Phys. Rev. B **76**, 195116 (2007).

[62] J. J. Kas, J. Vinson, N. Trcera, D. Cabaret, E. L. Shirley, and J. J. Rehr, J. Phys.: Conf. Ser. **190**, 012009 (2009).

[63] B. I. Lundqvist, Phys. Kondens. Mater. **6**, 206 (1967).

[64] L. Hedin and B. I. Lundqvist, J. Phys. C **4**, 2064 (1971).

[65] See Supplemental Material at http://link.aps.org/supplemental/10.1103/PhysRevB.107.115122 for the list of fitted parameters.